Journal of Nanobiotechnology

RESEARCH

Open Access

Myogenic nano-adjuvant for orthopedic-related sarcopenia via mitochondrial homeostasis modulation in macrophage-myosatellite metabolic crosstalk

Xudong Zhang[1,2†], Peng Zhang[1,2†], Yunliang Zhu[1†], Jiaqing Lou[4†], Peng Wu[5], Yingjie Wang[1], Zhengxi Wang[1], Quan Liu[1], Baoliang Lu[1], Qianming Li[1], Jiawei Mei[1*], Chen Zhu[1*], Wanbo Zhu[3*] and Xianzuo Zhang[1*]

Abstract

The decline in skeletal muscle mass and muscle strength linked to aging, also known as sarcopenia, is strongly associated with disability, traumatic injury, and metabolic disease in patients. Meanwhile, sarcopenia increases the risk of adverse orthopedic perioperative complications including implant dislocation, infection, loosening, and poor wound healing. Mitochondrial dyshomeostasis in the immune-myosatellite metabolic crosstalk is one of the major pathological factors in sarcopenia. To reduce the incidence of orthopedic perioperative complications in patients, we designed and developed a nano-adjuvant based on two-dimensional layer double hydroxide (LDH) for sustained improvement of systemic and orthopedic-related sarcopenia. Construction of MgAlCo-LDH@UA (MACL@UA) nano-adjuvant was performed by introducing cobalt in magnesium-aluminum LDH and further loading urolithin A (UA). The release of magnesium ions and UA promoted myocyte proliferation, angiogenesis and improved mitochondrial homeostasis. Al acted as an immunomodulatory adjuvant to enhance the metabolic crosstalk between macrophages and myosatellite cells, and prompted macrophage-derived glutamine nourishment. Animal experiments confirmed that vaccination with MACL@UA in systemic sarcopenia and intensive orthopedic perioperative vaccination with MACL@UA significantly enhanced quadriceps muscle mass in rats. This nano-adjuvant offers a solution for long-term improvement of sarcopenia and short-term significant reduction of orthopedic perioperative complications in patients, with promising prospects for clinical application and commercial translation.

†Xudong Zhang, Peng Zhang, Yunliang Zhu and Jiaqing Lou contributed equally to this work.

*Correspondence:
Jiawei Mei
meijiawei@mail.ustc.edu.cn
Chen Zhu
zhuchena@ustc.edu.cn
Wanbo Zhu
zhuwanbo@sjtu.edu.cn
Xianzuo Zhang
zhangxianzuo@ustc.edu.cn

Full list of author information is available at the end of the article

Keywords Orthopedic-related sarcopenia, Systematic sarcopenia, Myogenic nano-adjuvant, Mitochondrial homeostasis, Metabolic crosstalk

Introduction

Sarcopenia is one of the most serious consequences of age-related diseases and is characterized by loss of muscle mass and strength [1, 2]. Patients with sarcopenia suffer from a combination of serious health risks, including difficulty walking, susceptibility to falls and fractures [3]. For orthopedic surgery, more than half of sarcopenia patients are at risk for implant dislocation and infection due to decreased muscle tissue coverage [4]. Normal muscle content contributes to retarding the progression of degenerative diseases and reduces the incidence of postoperative complications [5].

As the most important organelles of muscle tissue, mitochondria are involved in a variety of cellular metabolic activities and play an integral role in the regulation of cell proliferation [6–10], senescence and apoptosis [11, 12]. The main pathological mechanism of sarcopenia involves mitochondrial hypofunction and dysfunction in myosatellites [13, 14]. The impairment and loss of mitochondrial function in muscle fibers is primarily due to deficient ATP synthesis as a result of the reduction of the mitochondrial tricarboxylic acid cycle and oxidative phosphorylation [15, 16]. The lack of ATP synthesis accompanied by intracellular oxidative stress triggers the deactivation of mitochondrial respiratory chain activity [17, 18], which results in the production of a large number of structurally abnormal mitochondria [19, 20], which is the hallmark of the onset of mitochondrial myopathy [21]. Therefore, restoring regulation of mitochondrial homeostasis in myosatellites is critical for muscle regeneration.

Suppressive immune modulation has a direct effect on muscle satellite cells [22]. Induced polarization of macrophages stimulates myosatellite cell proliferation and promotes myosatellite cell differentiation and proliferation as well as tissue vascularization [23, 24]. Among other things, the metabolic crosstalk of glutamine between macrophages and myosatellite cells has been investigated as a central regulator in the maintenance of muscle satellite cell homeostasis [25]. Macrophage-derived glutamine is utilized by myo-satellite cells and maintains satellite cell function [26, 27].

Urolithin A (UA) [28], an anti-aging agent, has been previously demonstrated to activate the AMPK-Sirt1 pathway for correction of the aberrant accumulation of mitochondria and promotion of mitochondrial recycling [29, 30]. The regulation of intracellular oxidative stress by the antioxidant effect of UA also provides favorable conditions for the regulation of mitochondrial homeostasis [31, 32]. Herein, we developed MgAlCo-LDH (MACL), a nano-adjuvant enriched with Mg, Al, and Co, and encapsulated UA in MACL to synthesize MACL@UA (Scheme 1). MACL@UA up-regulated the genes related to proliferation and myogenesis, inhibited myoblast senescence, and facilitated myoblast proliferation. The release of cobalt ions from MACL@UA facilitated the stabilization of Hif-1α, which in turn promoted angiogenesis. generation. The activation of AMPK and BCL-xl pathways by MACL@UA to regulate mitochondrial homeostasis was illustrated by RNA-seq. At the same time, MACL@UA enhanced the metabolic crosstalk between macrophages and myosatellite cells, and promoted the synthesis of glutamine and other cytokines to nourish myosatellite cells. In vivo experiments also demonstrated that muscle mass (55 ± 4.78 g, $n = 3$, $p < 0.05$) and grip strength (106 ± 5.13 g, $n = 3$, $p < 0.05$) were significantly reduced in the dexamethasone (DX) group compared to the control group, and that MACL@UA could be used for long-term improvement of sarcopenia in patients. More importantly, inoculation of MACL@UA in generalized sarcopenia and intensive orthopedic perioperative inoculation of MACL@UA significantly enhanced the muscle mass and muscle viability of quadriceps muscle in rats, which provides a new idea to avoid orthopedic perioperative complications.

Results and discussion

Characterization of MACL@UA

As shown in Scheme 1, we first synthesized MACL by the co-precipitation method, followed by MACL@UA by the one-pot method. Scanning electron microscope (SEM) images showed that the MACL presented as polygonal flakes and lamellae with dimensions mostly in the range of 600–1000 nm (Fig. 1a). Transmission electron microscopy (TEM) as well as Energy Dispersive Spectroscopy (EDS) elemental mapping revealed a homogeneous distribution of Mg, Al, and Co (Fig. 1b). Subsequently, the morphology and size of MACL were observed using atomic force microscopy (AFM), which confirmed that the MACL is a polydeformed lamellar structure with a thickness of about 1–1.5 nm (Fig. 1c). The particle sizes of the MACL and the MACL@UA were determined by a dynamic laser light scattering (DLS) analyzer, and the results were almost in good agreement with those observed by the electron microscope (Fig. 1d). We performed stability tests on MACL@UA for 7 days. The particle size of MACL@UA was stable between 650 and 780 nm and the zeta potential was stable between 6.29 and 9.51 mV (Fig. 1e). The small-angle X-Ray diffraction (XRD) patterns are shown in Fig. 1f. The MACL patterns

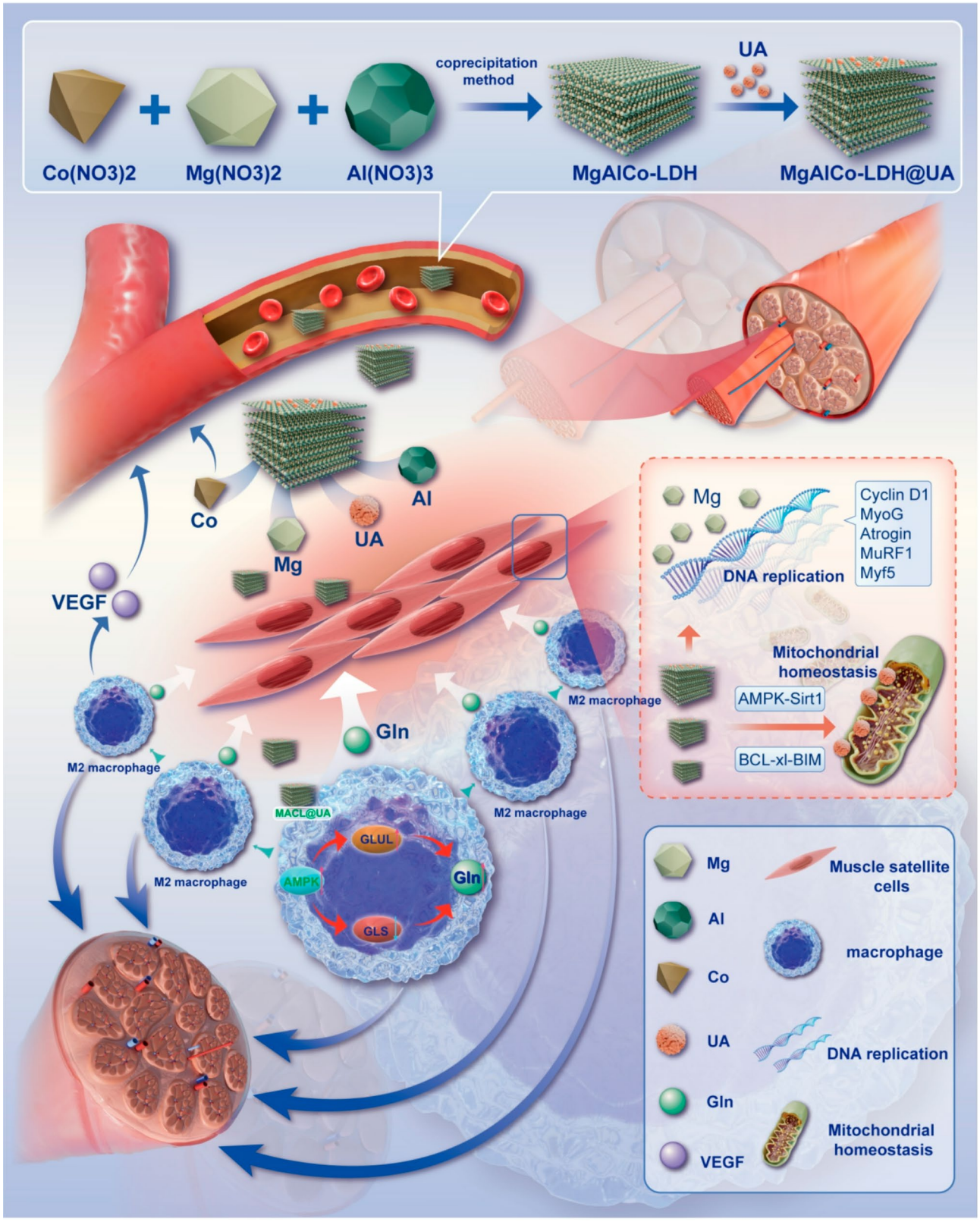

Scheme 1 Procedure in the synthesis of MACL@UA; MACL@UA promotes myogenesis by regulating mitochondrial homeostasis as well as modulating metabolic crosstalk between macrophages and myosatellite cells

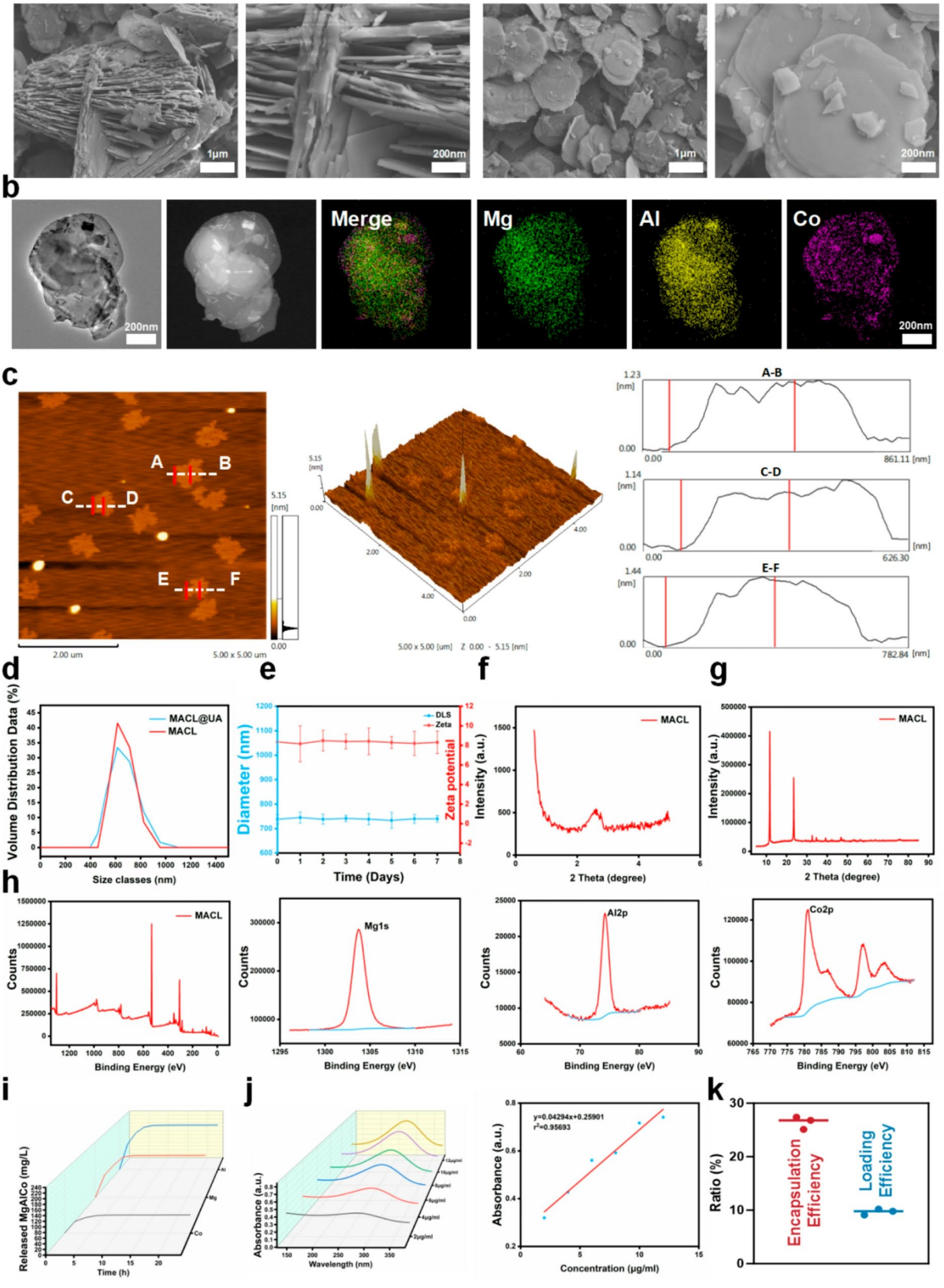

Fig. 1 (See legend on next page.)

(See figure on previous page.)

Fig. 1 Characterization of MACL and MACL@UA. **a**) SEM images of MACL. Scale bar, 1 μm and 200 nm. **b**) TEM and EDS mapping results of MACL. Scale bar, 200 nm. **c**) AFM images of MACL and thickness measurements. Scale bar, 200 μm. **d**) Particle size distributions of MACL. **e**) Zeta potentials of MACL andMACL@UA. **f**) Small-angle XRD of MACL. **g**) Wide-angle XRD of the MACL. **h**) XPS spectra of MACL. **i**)Release patterns of Mg/Al/Co from MACL within 24 h. **j**)The UV-Vis absorption at 289 nm and the standard curve of UA. **k**)HPLC-determined encapsulation and loading efficiency of UA. ($n = 3$, $^{*}p < 0.05$, $^{**}p < 0.01$, $^{***}p < 0.001$, $^{****}p < 0.0001$. Data are expressed in mean ± SD.)

show diffraction peaks at 2θ of 0.6°, 2.64°, and 4.94°. The wide angle XRD pattern showed diffraction peaks at 2θ of 11.72°, 23.52°32.62°, 34.68°, 39.3°, and 48.1°, indicating the successful synthesis of MACL (Fig. 1g). The presence of Mg1s, Al2p, and Co2p binding energies in the XPS pattern indicated the synthesis of MACL (Fig. 1h). ICP was used to detect the release of Mg, Al, and Co from MACL@UA (Fig. 1i). The ability of MACL@UA to release large amounts of Mg, Al, and Co lays the foundation for its ability to contribute to myogenesis and angiogenesis. Thereafter, we immersed MACL@UA in PBS to study UA release by UV-Vis absorbance of the supernatant at 280 nm (Fig. 1j). The UV-Vis standard curves for UA were determined from the peak absorbance at different the UV-Vis standard curves for UA were determined from the peak absorbance at different concentrations (Fig. 1j). We determined the encapsulation efficiency and loading efficiency of UA in MACL@UA using HPLC, which were 26.4% and 9.8%, respectively (Fig. 1k).

Cell Counting Kit-8 (CCK-8) assay was performed assessing the biosafety of MACL@UA. C2C12 cells and Human umbilical vein endothelial cells (HUVECs) were co-cultured with DX for 12 h, respectively, and then sequentially added with different concentrations of MACL@UA (0, 50, 100, 150, 200, 250, 250, 300, 350, 400, 500 μg/ml)(Figure S1a). As shown, the growth of C2C12 cells was inhibited when the concentration of MACL@UA exceeded 350 μg/ml. When the concentration of MACL@UA was located between 100 and 250 μg/ml, it was growth-promoting for C2C12 cells after DX intervention (Figure S1b). The optimal growth-promoting concentration for HUVECs was located between 150 and 250 μg/ml. For macrophages, MACL@UA possessed toxicity when its concentration exceeded 400 μg/ml (Figure S1c). We also examined ER stress-related metrics in C2C12 cells and MUSCs and showed that MACL@UA did not cause ER stress (Figure S2). The results of the hemolysis assay showed that the hemolysis rate was less than 5% at concentrations of MACL@UA less than 300 μg/ml(Figure S3). Based on these biocompatibility tests, 200 μg/ml was selected as our therapeutic concentration. We also examined ER stress-related metrics in C2C12 cells and MUSCs and showed that MACL@UA did not cause ER stress.

MACL@UA reverses DX-induced myocyte senescence and promotes myocyte and vascular proliferation

To investigate the regulatory effects of MACL@UA on myocyte senescence and proliferation, C2C12 cells were selected as classical myoblasts for culture and differentiation, and dexamethasone (DX) was selected as a negative control. Four groups were established, including Control, DX, DX + MACL, and MACL@UA. Previous studies have shown that Mg^{2+} and Co^{2+} have the ability to up-regulate proliferation-related genes [33–35]. The results of inductively coupled plasma (ICP) also demonstrated that MACL@UA was able to release sufficient Mg^{2+}. The results of RT-PCR illustrated that MACL@UA was able to up-regulate proliferation (*Cyclin D1*) as well as myogenesis (*MyoG*, *Murf1*, *Myf5*)-related genes (Fig. 2a) [36–38]. The results of Western blot also showed that MACL@UA promotes the expression of myogenesis-related proteins(Figure S4) [39, 40]. Encouraged by the up-regulation of the expression of proliferative muscle-forming related genes, the scratch assay was used to verify the effect of MACL@UA on myoblast proliferation. As shown in Fig. 2b, the addition of DX increased the scratch spacing and the addition of MACL@UA reversed the effect of DX. The results of the cell proliferation assay showed that MACL@UA not only reversed the toxicity of DX, but also promoted the proliferation of myoblasts compared to the control group (Fig. 2c, S5). Myotube formation is a hallmark of myocyte proliferation, and increased expression of myosin heavy chain gene (*MYH7*) implies the formation of new myotubes. As shown in Fig. 2d and Figure S6, MACL@UA not only reversed the DX-induced myotube reduction, but also increased myotube formation compared to the control group. The anti-aging efficacy of UA has been previously demonstrated. We then performed immunofluorescence staining of the different treatment groups, and the MACL@UA group down-regulated p53 and P16, which are indicators of aging, compared to the DX group (Fig. 2e, S7).

Previous studies have demonstrated that cobalt ions have a stabilizing effect on the hypoxia-inducible factor (Hif-1α) [41, 42]. Therefore, cobalt ions may have a promotional effect on angiogenesis. ICP was used to detect the amount of cobalt ions released from MACL@UA. Adequate cobalt ion release provided the basis for us to investigate the effect of MACL@UA on angiogenesis. RT-PCR results all demonstrated that MACL@UA upregulated Hif-1α (Figure S8). HUVECs were used for tube-forming experiments. As shown in Fig. 2g-h, the

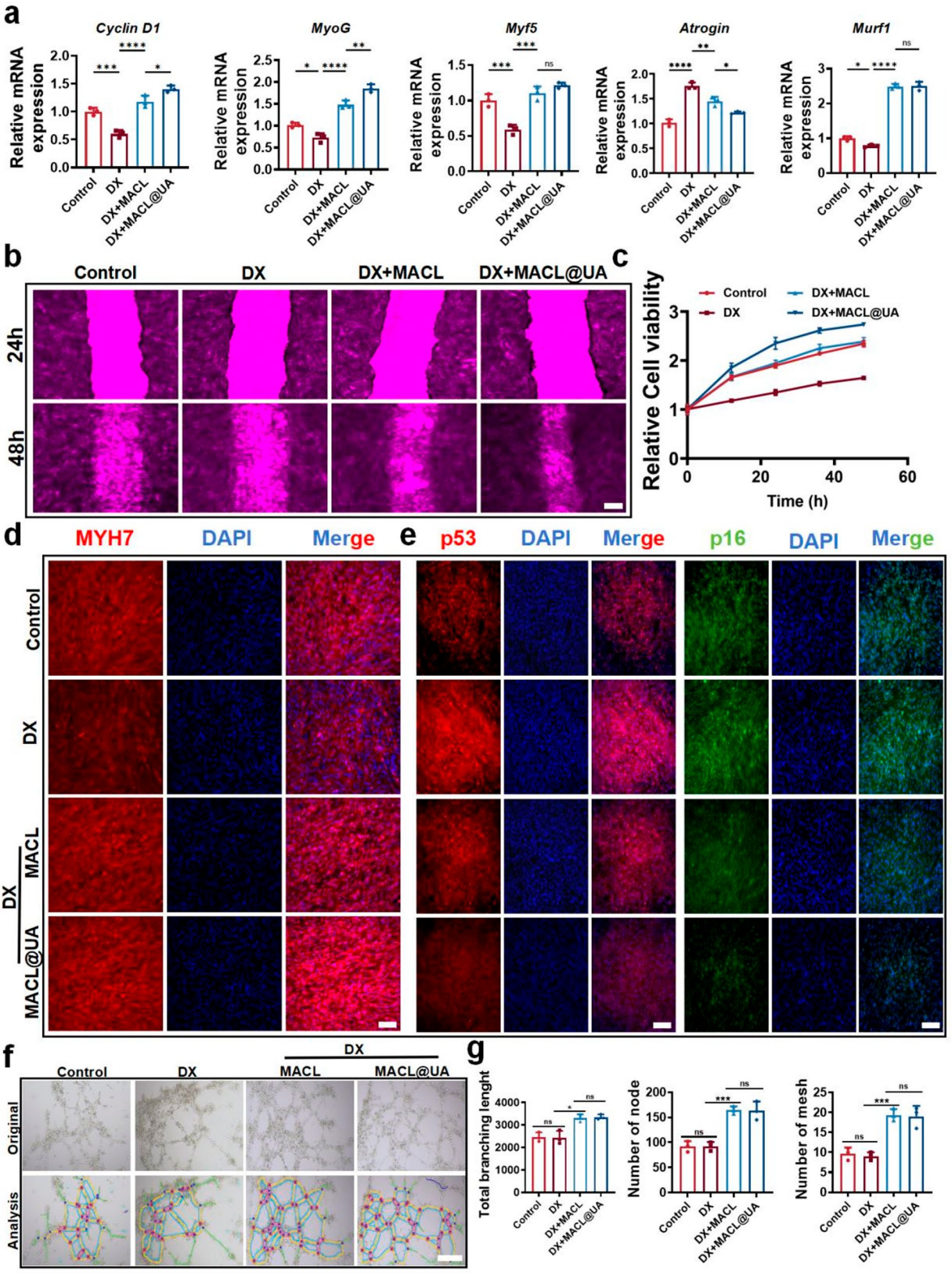

Fig. 2 (See legend on next page.)

(See figure on previous page.)

Fig. 2 MACL@UA promotes myogenesis and vasculogenesis. **a**) Myogenesis and proliferation-associated mRNA expression in C2C12 cells. **b**) Results of scratch assay of C2C12 cells after different interventions. Scale bar, 200 μm. **c**) Proliferation curve of C2C12 cells. **d**) Immunofluorescence staining images of Myh7, an indicator of myotube formation. Scale bar, 100 μm. **e**) Immunofluorescence staining images of p53/p16, an indicator of senescence. Scale bar, 100 μm. **f**) Angiogenesis of HUVECs after different interventions. Scale bar, 200 μm. **g**) Quantitative analysis of total branch lenght/number of node/number of mesh results. ($n = 3$, *$p < 0.05$, **$p < 0.01$, ***$p < 0.001$, ****$p < 0.0001$. Data are expressed in mean ± SD.)

MACL@UA group was superior to the control group in terms of total branch length, number of nodes, and amount of mesh. The cell proliferation assay also supported this result (Figure S9).

By analyzing the results of the above experiments, we found that MACL was also able to promote the proliferation and delay the senescence of C2C12. This is most likely by virtue of its excellent ability to release Mg^{2+} and Co^{2+}. The ability of Mg^{2+} and Co^{2+} to promote proliferation has also been confirmed in other previous studies [37, 38, 43]. MACL@UA has a better therapeutic effect compared to MACL, most likely because UA both enhances Mg^{2+} and Co^{2+} functions and regulates C2C12 proliferation through other mechanisms. This needs to be further explored.

MACL@UA promotes AMPK and BCL-xl pathways and regulates mitochondrial homeostasis genes

To further investigate the mechanism of MACL@UA promoting myocyte proliferation, we sequenced the whole genome of C2C12 cells from different treatment groups. Principal component analysis and correlation analysis demonstrated consistent within- group deviations, validating the RNA-seq data (Figure S10). Volcano plots showed a total of 427 genes up-regulated and 529 genes down-regulated (Figure S11). Pathway enrichment analysis showed that after MACL@UA intervention, mitotic DNA replication initiation, DNA repair, mitochondrion, ATP binding, AMPK signaling pathway and formation of BAX/ BCL-xl complex and other pathways were upregulated (Fig. 3a, S12). The results of gene heat map analysis further confirmed that MACL@UA promotes the expression of repair- and proliferation-related genes (Fig. 3b). The results of GSEA showed that mitochondrial inner membrane, mitochondrial respiratory chain complex I, oxidative phosphorylation, ATP hydrolysis activity and other pathways were upregulated (Fig. 3c, S13). The RNA-sq results demonstrate that MACL@UA not only upregulates mitotic as well as proliferation-related genes, but also promotes pathways that favor mitochondrial homeostasis (Fig. 3d). Previous studies have shown that the AMPK-Sirt1-PGC1α axis as well as the BCL-xl-Bim axis are of great significance for the regulation of mitochondrial homeostasis. Mitochondrial stability is inextricably linked to myocyte proliferation and apoptosis [44–47]. Encouraged by the RNA-sq results, we then validated the above two pathways. As shown in Fig. 3e, addition of MACL@UA reversed the down-regulation of DX for the AMPK-Sirt1-PGC1α axis as well as the BCL-xl-Bim axis, and up-regulated these pathways compared to controls. Meanwhile, DX-induced up-regulation of Drp 1 expression and down-regulation of Mfn 1 expression implies enhanced mitochondrial division, which is reversed by MACL@UA. The mRNA expressions of mitochondria motility mediator (Miro) and mitochondrial DNA (mtCO2 and mtND1) were notably changed after MACL@UA treatment. These findings altogether proved that MACL@UA could help retain mitochondrial dynamics and alleviate mitochondrial dysfunction induced by DX. (Fig. 3f) [48–51]. This result was further confirmed in Western blotting experiments (Fig. 3g-h, S14). In conclusion, MACL@UA was able to regulate mitochondrial homeostasis by up-regulating the AMPK and BCL-xl pathways and laid the foundation for the improvement of mitochondrial function.

MACL@UA improves C2C12 intracellular environment and enhances mitochondrial function

Regulation of mitochondrial homeostasis is critical for alleviating myocyte injury and promoting myocyte proliferation. Elevated ROS levels due to various factors are one of the main triggers of mitochondrial homeostatic imbalance [52]. High levels of ROS are not only the cause of mitochondrial homeostasis, but also interfere with the repair of mitochondrial homeostasis. Previous studies have shown that ROS inhibit the AMPK-related pathway and thus interfere with the repair of mitochondrial homeostasis [53–55]. Therefore, removing ROS from the cellular microenvironment not only inhibits cellular damage, but also removes obstacles to mitochondrial repair. Intracellular oxidative stress induced by high levels of ROS is one of the important hallmarks of mitochondrial dysfunction [56, 57]. Subsequently, we examined several oxidative stress markers, including superoxide dismutase (SOD) activity [58], ROS [32, 50], and malondialdehyde (MDA) [59, 60]. Addition of MACL@UA increased SOD activity and laid the foundation for ROS scavenging (Fig. 4a). DCFH-DA was used to label intracellular ROS, and after the intervention of MACL@UA, the intracellular ROS content of C2C12 was significantly reduced compared with that of the DX group (Fig. 4b, S15). Meanwhile, the results of malondialdehyde (MDA) content further confirmed the clearance of ROS (Fig. 4c). This shows that MACL@UA is highly effective in altering intracellular oxidative stress. ATP is central to energy metabolism and supports almost all

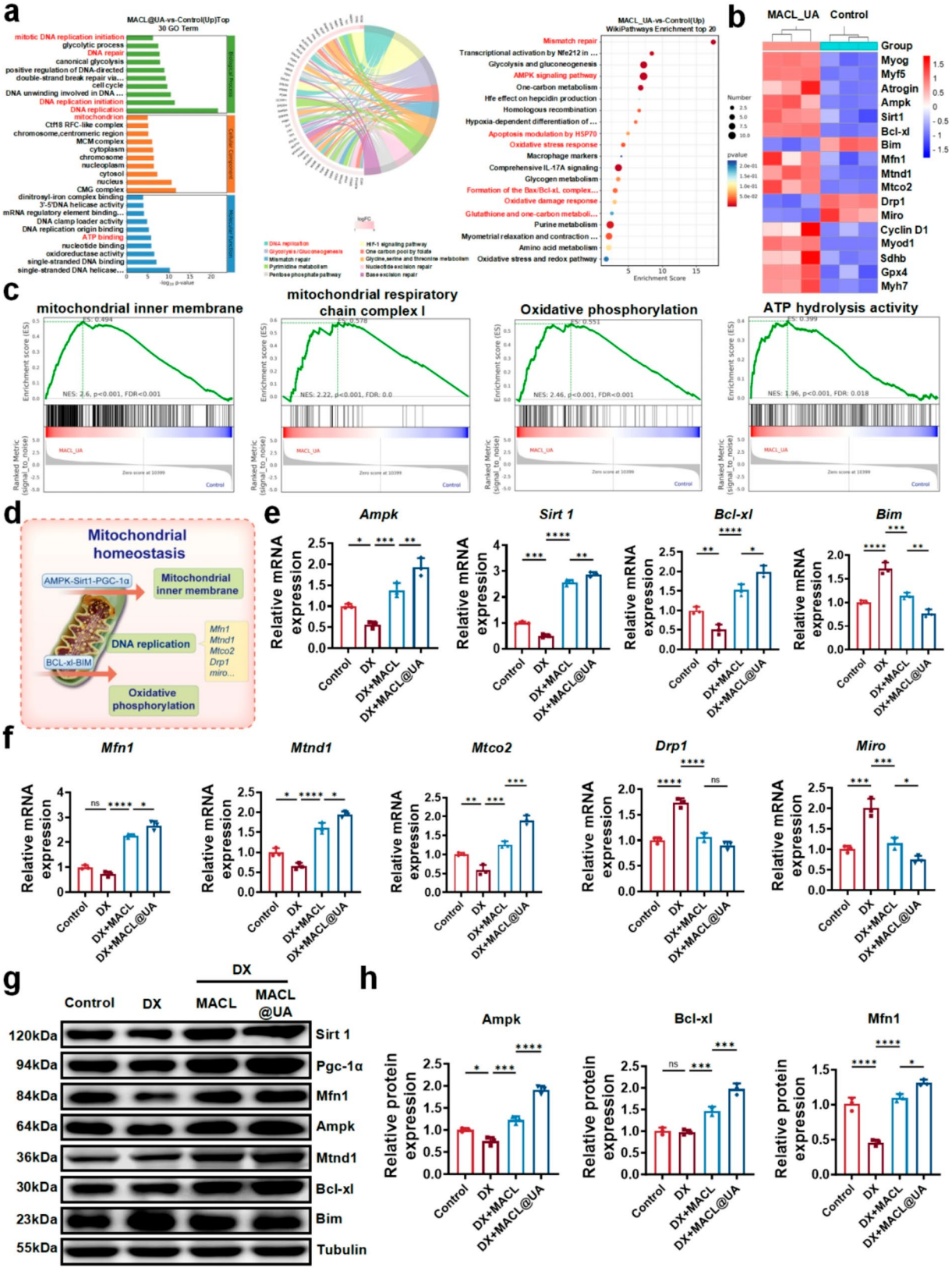

Fig. 3 (See legend on next page.)

(See figure on previous page.)

Fig. 3 Exploration of the Mechanism of MACL@UA to Promote Myogenesis. **a**) GO/KEGG/Wikipathways enrichment of up-regulated genes. **b**) Heat map analysis of genes for muscle formation as well as mitochondrial dynamics. **c**) Gene set enrichment analysis (GSEA) of mitochondrial inner membrane, mitochondrial respiratory chain complex I, oxidative phosphorylation and ATP hydrolysis activity. **d**) Schematic diagram of mitochondrial homeostatic regulation. **e**) Expression of mRNA related to AMPK-Sirt1 pathway and BCL-xl-Bim pathway in C2C12 cells. **f**) Related expression of mRNA of mitochondrial dynamic in C2C12 cells. **g**) Western blot results of the expression of mitochondrial homeostasis-related protein. **h**) Corresponding quantitative analysis of mitochondrial homeostasis-related protein. ($n = 3$, $^{*}p < 0.05$, $^{**}p < 0.01$, $^{***}p < 0.001$, $^{****}p < 0.0001$. Data are expressed in mean ± SD.)

types of cellular activities, and the stability of ATP synthesis is one of the hallmarks of mitochondrial homeostasis. Our RNA sequencing results show that MACL@UA promotes the upregulation of oxidative phosphorylation, suggesting stable ATP synthesis. This result is also consistent with our subsequent Western blotting experiments (Figure S16). As shown in Fig. 4d, the addition of MACL@UA significantly increased ATP synthesis compared to the control and DX groups. Stabilization of ATP synthesis provides energetic support for mitochondrial function and repair. To assess mitochondrial function after MACL@UA intervention, we assayed mitochondrial respiratory chain complex activity. As shown in Fig. 4e, the addition of MACL@UA greatly improved the mitochondrial respiratory chain complex activity impaired by DX. Mitochondrial membrane potential (MMP) is an important parameter of mitochondrial outer membrane permeability and integrity [61–63]. Therefore, JC-1 was used for immunofluorescence staining to assess mitochondrial membrane integrity. The DX group showed a decrease in fluorescence intensity of JC-1 aggregates (red) and an increase in fluorescence intensity of JC-1 monomers (green), suggesting a decrease in MMP and a disruption of mitochondrial membrane integrity (Fig. 4f). Addition of MACL@UA promoted the production of JC-1 aggregates and restored the JC-1 monomer/aggregate ratio, thereby stabilizing mitochondrial membrane integrity. The regulation of MMP by MACL@UA is critical for the inhibition of cellular senescence and death. Oxygen consumption rate (OCR) is often used to reflect cellular mitochondrial function [64, 65]. Measurements of OCR showed that basal respiration was impaired by the addition of DX and improved after MACL@UA intervention. MACL@UA significantly ameliorated the reduction in maximal respiration induced by FCCP after the addition of DX (Fig. 4g). In addition, MACL@UA enhanced ATP-associated respiration. The impaired proton-leak caused by DX was also reversed to some extent by MACL@UA (Fig. 4h). The regulation of OCR by MACL@UA also underlies the promotion of myocyte proliferation. Transmission electron microscopy images showed that DX induced a decrease in mitochondrial density, cristae disruption and membrane rupture. MACL@UA ameliorated this morphological damage and increased mitochondrial density (Fig. 4i).

Briefly, MACL@UA has a superior effect on regulating mitochondrial homeostasis compared to MACL. Due to the grafting of UA, MACL@UA removes high levels of ROS within the microenvironment, altering the intracellular oxidative stress environment and blocking the causative agent of mitochondrial homeostatic imbalance. ROS scavenging enhances the regulation of the AMPK-sirt1-PGC1α axis and the BCL-xl-Bim axis. It also promotes ATP synthesis by facilitating oxidative phosphorylation, which provides energy for mitochondrial function and repair. Meanwhile, the stabilization of ATP synthesis also provided energy for myocyte proliferation. The results of MMP, OCR and TEM suggested the restoration of mitochondrial function, which was indirect evidence that MACL@UA alleviated myocyte injury.

Al as a muscle-forming immune adjuvant enhances the trophic effect of macrophages on myosatellite cells

In recent years, more and more studies have shown that macrophages are indispensable in muscle regeneration [66, 67]. Factors such as *Arg-1*, *IL-10*, *IGF-1*, *VEGF* secreted by M2-type macrophages can inhibit inflammation and promote myofibril formation, vascular regeneration, and tissue reconstruction [68, 69]. UA-induced macrophage polarization to M2-type has been demonstrated in previous studies [70, 71]. Al as an immunoadjuvant has been applied to various fields such as antiviral, antibacterial, and antitumor, while studies in myogenesis are not clear. To explore the effect of Al on immune regulation, four experimental groups were established, including Control, DX, MCL@UA, and MACL@UA. The results of RT-PCR showed that MCL@UA promoted the up-regulation of genes such as macrophage *Arg-1*, *IL-10*, *IGF-1*, and *VEGF*, which was further strengthened by Al-containing MACL@UA (Fig. 5a). The results of Western blotting also showed that Al has a reinforcing role in the regulation of macrophages by MACL@UA (Fig. 5b).

The metabolic interactions between macrophages and myosatellite cells are not known. However, macrophage-derived glutamine (Gln) has been shown to promote myosatellite cell activation and muscle regeneration [72, 73]. Activation of the AMPK pathway has a critical role in Gln secretion [73]. Encouraged by the activation of the AMPK pathway by MACL@UA for C2C12 cells, we examined the expression of AMPK in macrophages using RT-PCR and Western blotting. As shown in Fig. 5a-b, MACL@UA upregulated the macrophage AMPK pathway, whereas MCL@UA without Al was slightly less effective. Subsequently, we examined the

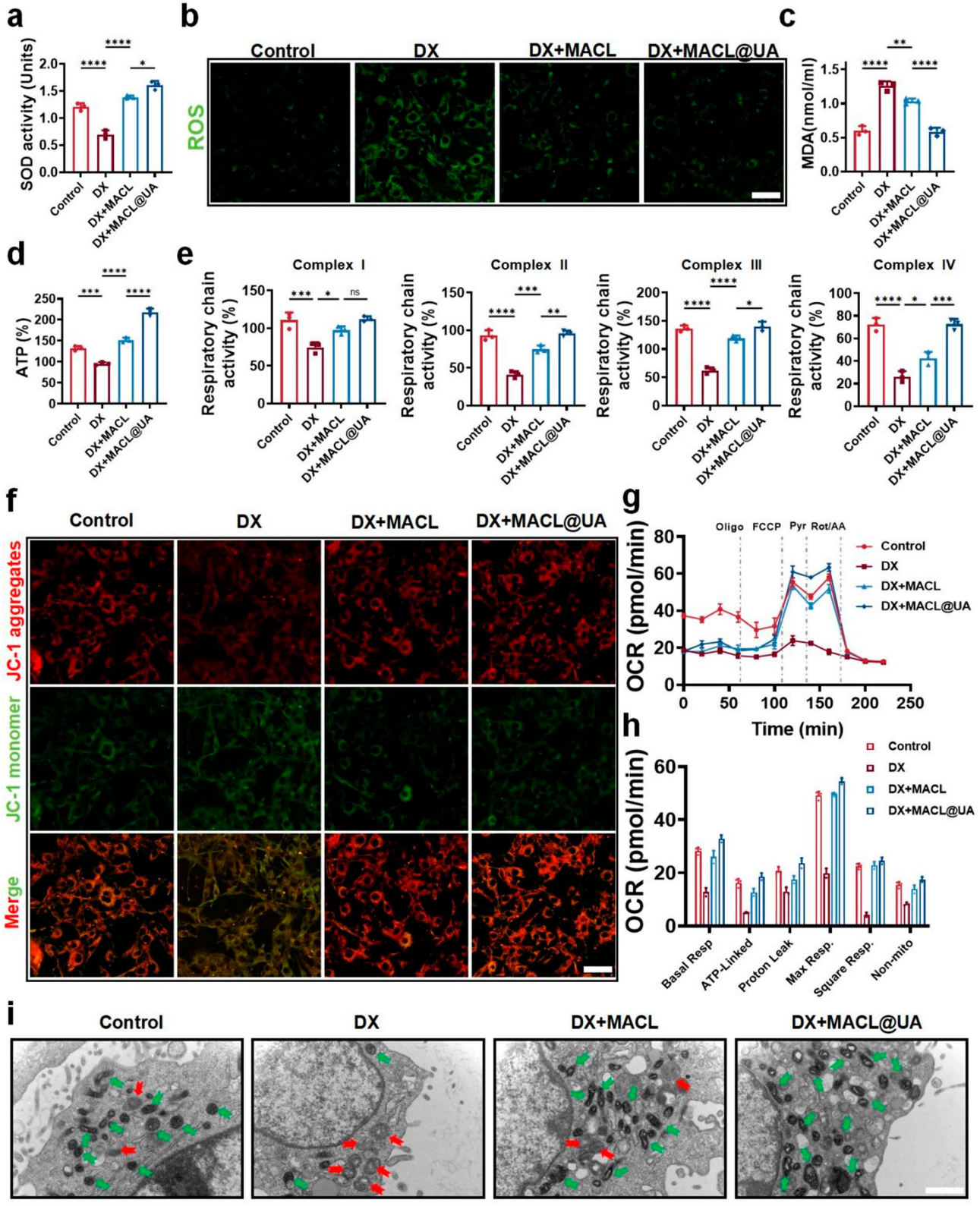

Fig. 4 (See legend on next page.)

(See figure on previous page.)

Fig. 4 MACL@UA improved mitochondrial function. **a**) SOD activity in C2C12 cells after different treatments. **b**) Fluorescence images of intracellular ROS using DCFH-DA probe with various interference. Scale bar, 200 μm. **c**) MDA content in C2C12 cells after different treatments. **d**) Intracellular ATP content of C2C12 cells. **e**) Respiratory chain complex activity of C2C12 cells after incubation with various treatments. **f**) JC-1 staining image of the inner mitochondrial membrane. Scale bar, 200 μm. **g**) Representative oxygen consumption rate (OCR) curves. **h**) OCR quantification. **i**) TEM images of C2C12 cells mitochondria in various groups. Red arrows represent swollen mitochondria and green arrows represent intact mitochondria. Scale bar, 10 μm. ($n = 3$, $^{*}p < 0.05$, $^{**}p < 0.01$, $^{***}p < 0.001$, $^{****}p < 0.0001$. Data are expressed in mean ± SD.)

levels of glutaminase (GLS), and MACL@UA significantly decreased the levels of GLS relative to the other groups (Fig. 5c). Subsequently, we found in the Gln content assay that the MACL@UA group had higher Gln content than the other groups (Fig. 5c). Immunofluorescence staining showed that the addition of MACL@UA significantly increased glutamine synthase (GLUL) secretion relative to the MCL@UA and control groups (Fig. 5d). This also provided the basis for the large amount of Gln secreted by macrophages. Finally, we collected macrophage supernatants after different treatments and added them to MuSCs for culture. JHU was selected as a Gln inhibitor for assessing cell proliferation by flow cytometry and EDU was used to label proliferating cells. As shown in Fig. 5e-f, cell proliferation was evident in the group with the addition of MACL@UA-treated macrophage supernatants, while proliferation was affected in the group with the addition of JHU.

In conclusion, MACL@UA was able to regulate the polarization of macrophages to M2 type and secrete factors such as *Arg-1*, *IL-10*, *IGF-1*, *VEGF*, which promote muscle regeneration and angiogenesis. MACL@UA was also able to activate the AMPK pathway to promote the secretion of Gln and thus nourish myosatellite cells. Our results also indicated that Al could enhance the regulatory effect of MACL@UA on macrophages.

In vivo treatment of systemic sarcopenia with MACL@UA

Encouraged by the in vitro experiments, we then explored the in vivo efficacy of MACL@UA. As shown in the Fig. 6a, systemic sarcopenia was simulated by injecting rats with a high dose of DX for 15 consecutive days, and four groups were established including Control, DX, DX + MACL, and DX + MACL@UA. We set the day the model was built as day 0, and treated the rats by intravenous injection on this day. The quadriceps muscle was taken on days 0, 7, and 14 as a representative for histologic analysis to assess the in vivo efficacy of MACL@UA. By measuring muscle width and leg circumference on days 0 and 14, we found that the muscle content of rats treated with MACL@UA increased significantly compared to DX group (Fig. 6b, S17, S18). At the same time, we weighed the removed muscles, and the muscle mass was higher in the MACL@UA group than in the other groups (Fig. 6c). We also weighed the rats during this period, and the rats in the MACL@UA group showed a significant increase in body weight compared to the DX group (Figure S19), a result that was consistent with the muscle width and leg circumference measurements, further demonstrating the excellent efficacy of MACL@UA in vivo. H&E staining of quadriceps muscle was taken on the 14th day, and it was found that the muscle tissues in the DX group were mostly degraded and necrotic, whereas the muscle tissues in the MACL@UA treatment group were rich in muscle tissue content and accompanied by the formation of blood vessels (Fig. 6d). Immunohistochemical staining of CD31 also further proved that MACL@UA had the excellent ability to promote the generation of blood vessels (Figure S20), which provided a favorable condition for the regeneration of the muscles. Myhc, an important indicator of myotube formation, was also used for immunofluorescence staining, a result that also supports the ability of MACL@UA to be used in the treatment of sarcopenia (Fig. 6e).

Immunofluorescence staining and immunohistochemical staining were also used to explore the mechanism by which MACL@UA promotes myogenesis in vivo. AMPK and anti-apoptotic BCL-xl proteins were significantly up-regulated after MACL@UA treatment (Fig. 6f, S21), which suggests that the mechanism by which MACL@UA promotes myogenesis is basically the same as that in vitro. The structure and morphology of mitochondria in muscle tissue were observed by TEM, and the mitochondria in the DX group were mostly swollen with incomplete mitochondrial membranes, while the mitochondria in the MACL@UA treated group were not only structurally intact, but also increased in number (Fig. 6g).

Finally, the motor function of rats was assessed by grip test experiment and treadmill experiment. The rats showed a significant increase in grip strength on day 7, and the grip strength of the MACL@UA group was close to 350 g on day 14, whereas that of the DX group was only 290 g (Fig. 6h). The treadmill test also showed that the MACL@UA treatment significantly increased the distance and time of the rats' exercise (Fig. 6i-j). In short, the complications of sarcopenia leading to dyskinesia can be significantly improved after MACL@UA treatment.

MACL@UA for perioperative treatment of orthopedic-related sarcopenia

Patients with systematic sarcopenia may suffer from complications such as difficulty in mobility [74], wound healing [75], and infection after orthopedic surgery. Therefore, orthopedic perioperative treatment of patients

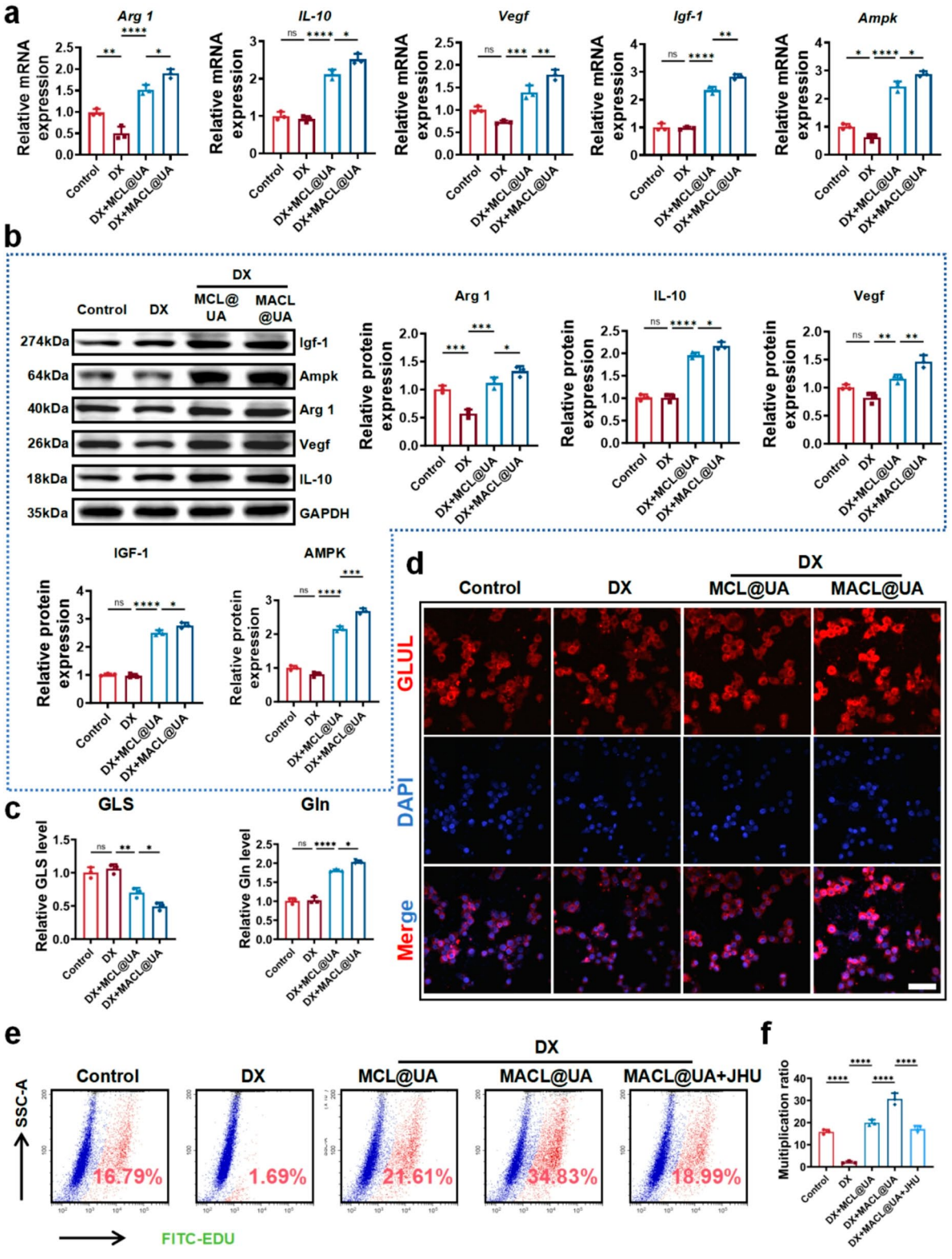

Fig. 5 MACL@UA regulates metabolic crosstalk in macrophages and myosatellite cells. **a**) Expression of mRNA of macrophage M2-marker. **b**) Western blot results of the expression and quantitative analysis of macrophage M2-marker protein. **c**) Macrophage intracellular levels of GLS and Gln after different interventions. **d**) Fluorescence staining images of GLUL. Scale bar, 100 μm. **e**) EDU flow analysis of macrophage supernatants after co-culture with MuSCs after different interventions. **f**) Quantitative analysis of EDU flow analysis. ($n = 3$, $^{*}p < 0.05$, $^{**}p < 0.01$, $^{***}p < 0.001$, $^{****}p < 0.0001$. Data are expressed in mean ± SD.)

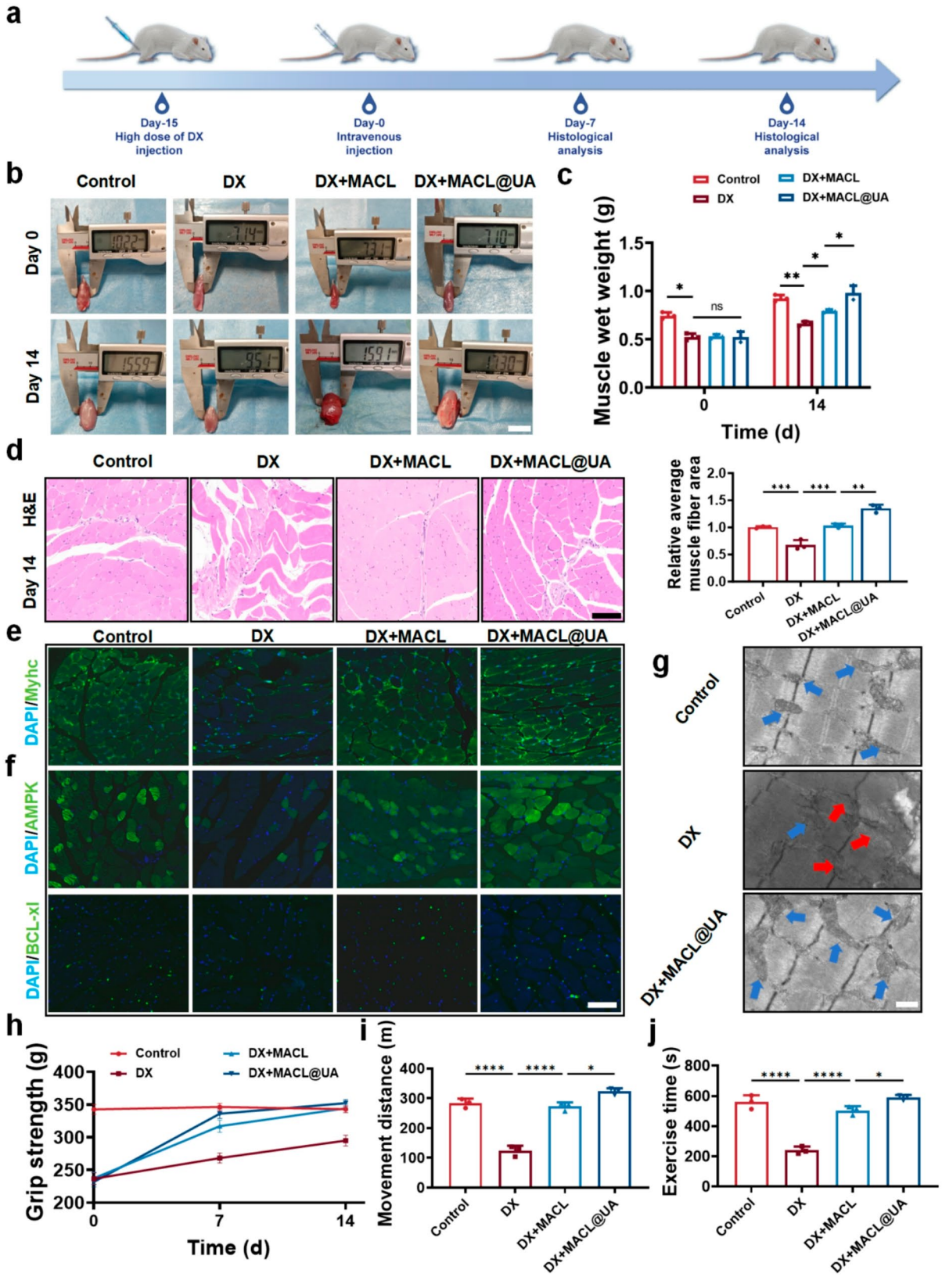

Fig. 6 (See legend on next page.)

(See figure on previous page.)

Fig. 6 MACL@UA treat systemic sarcopenia in vivo. **a**) Establishment of myasthenia gravis model and treatment steps. **b**) Measurement of muscle width of different treatment groups on day 0 and 14. Scale bar, 20 mm. **c**) Muscle wet weight of rats in different treatment groups on day 0 and 14. **d**) H&E staining images of muscles and quantitative analysis of mean muscle fiber area of different treatment groups on day 14. Scale bar, 200 μm. **e**) Immunofluorescence staining images of myotubular markers of different treatment groups. 200 μm. **f**) Immunofluorescence staining images of AMPK and BCL-xl. Scale bar, 200 μm. **g**) Immunofluorescence staining images of different treated muscle mitochondrial TEM images. Red arrows represent swollen mitochondria and blue arrows represent intact mitochondria. Scale bar, 10 μm. **h**) Grip force curves of rats after different treatments. **i**) Distance traveled and exercise time of rats measured by treadmill experiments. ($n = 3$, *$p < 0.05$, **$p < 0.01$, ***$p < 0.001$, ****$p < 0.0001$. Data are expressed in mean ± SD.)

with systematic sarcopenia is crucial to avoid complications. Al has long been used as a vaccine adjuvant for antitumor, antiviral, and antibacterial applications, and whether it can be used as an adjuvant for muscle-forming vaccines remains to be explored. As shown in Fig. 7a, systematic sarcopenia was simulated by injecting rats with a high dose of DX on 15 consecutive days. The day the model was built was designated as day 0, and an intravenous injection of MACL@UA was administered, similar to vaccination. We simulated orthopedic surgery in rats on day 7 to establish a perioperative model of orthopedic-related sarcopenia, and intensive treatment with local injection of MACL@UA was performed on day 10. Thus, five groups were established, including Control, DX, DX + MCL@UA (without Al), DX + MACL@UA, and DX + MACL@UA@LI (with the addition of local injection on day 10). Measurements of leg circumference and body weight of rats in the five groups revealed that the body weight and leg circumference of the MACL@UA-containing treatment group were higher than those of the MCL@UA group and the DX group (Fig. 7b, S22-24). Muscle wet weight was higher in the MACL@UA@Li group than in the other groups (Fig. 7c). Leg circumference and body weight of the MACL@UA@LI group were even significantly higher than those of the Control group. The results of H&E staining showed that muscle fibers were more intact and abundant in the MACL@UA group compared to the MCL@UA group, suggesting that the presence of Al enhanced the role of MACL@UA in promoting muscle production (Fig. 7d). The MACL@UA@LI group had the best treatment outcome with the richest myofibers accompanied by angiogenesis. Masson staining and CD31 immunohistochemical staining results similarly confirmed that MACL@UA@LI promoted muscle repair and massive blood vessel formation (Fig. 7e, S25). By measuring the Mg^{2+} levels in peripheral blood, we found that after day 14, the MACL@UA group had higher peripheral hematological Mg^{2+} levels than the MCL@UA group (Figure S26). This phenomenon suggests that the presence of Al prolongs the residence time of MACL@UA in the body, thus providing favorable conditions for perioperative treatment. This shows that rats suffering from dystrophic sarcopenia can achieve a good muscle-forming efficacy by intravenously injecting vaccine-like MACL@UA before surgery. What's more, local supplementation of MACL@UA at the surgical site after surgery can strengthen the effect of preoperative treatment. Geriatric sarcopenia is a systemic disease for which intravenous therapy is undoubtedly the best option, and MACL@UA, with its excellent in vivo residency, provides the rationale for long-term chronic therapy of sarcopenia. Local injections alone, while having a more efficient local therapeutic effect, lack a systemic therapeutic effect. Therefore, when confronted with the perioperative treatment of patients with systemic sarcopenia. The use of intravenous injection combined with local injection intensive treatment has absolute advantages. Intravenous injection can be used for chronic long-term treatment of senile generalized sarcopenia, and supplemented with local injection has good therapeutic effect on acute muscle loss caused by surgery.

Immunofluorescence staining and immunohistochemical staining were also used to investigate the mechanism of myogenesis, and MACL@UA treatment promoted the up-regulation of AMPK and BCL-xl (Fig. 7f, S27-28). TEM results showed that the mitochondria were more structurally and morphologically intact after treatment with MACL@UA (Fig. 7g).

For the assessment of motor function in rats, the grip test experiment and treadmill experiment were still used. The grip strength of rats injected with MACL@UA preoperatively was significantly higher (349 g), while the main strength of rats topically supplemented with MACL@UA on the 10th day was able to reach an astonishing 370 g (Fig. 7h). Similarly, the rats in the MACL@UA@LI group were ahead of the other groups in terms of the distance and time of the exercise (Fig. 7i-j). This shows that the perioperative treatment regimen of preoperative intravenous injection of MACL@UA combined with postoperative topical MACL@UA can significantly improve the postoperative locomotor activity of rats with dystrophic myasthenia gravis.

To assess the systemic effects of intravenous MACL@UA, we performed hematological analysis on mice. The routine blood results showed that MACL@UA did not alter the levels of various types of blood cells and platelets (Figure S29). Serum biochemical analysis showed that alanine aminotransferase, glutathione transaminase and creatinine were normal after MACL@UA injection (Figure S30). MuSCs and mature muscle cells were selected for our ER stress assay, and the results showed that MACL@UA does not induce ER stress in muscle tissue in rats (Figure S31). H&E staining of major organs (including heart, liver, spleen, lungs and kidneys) showed

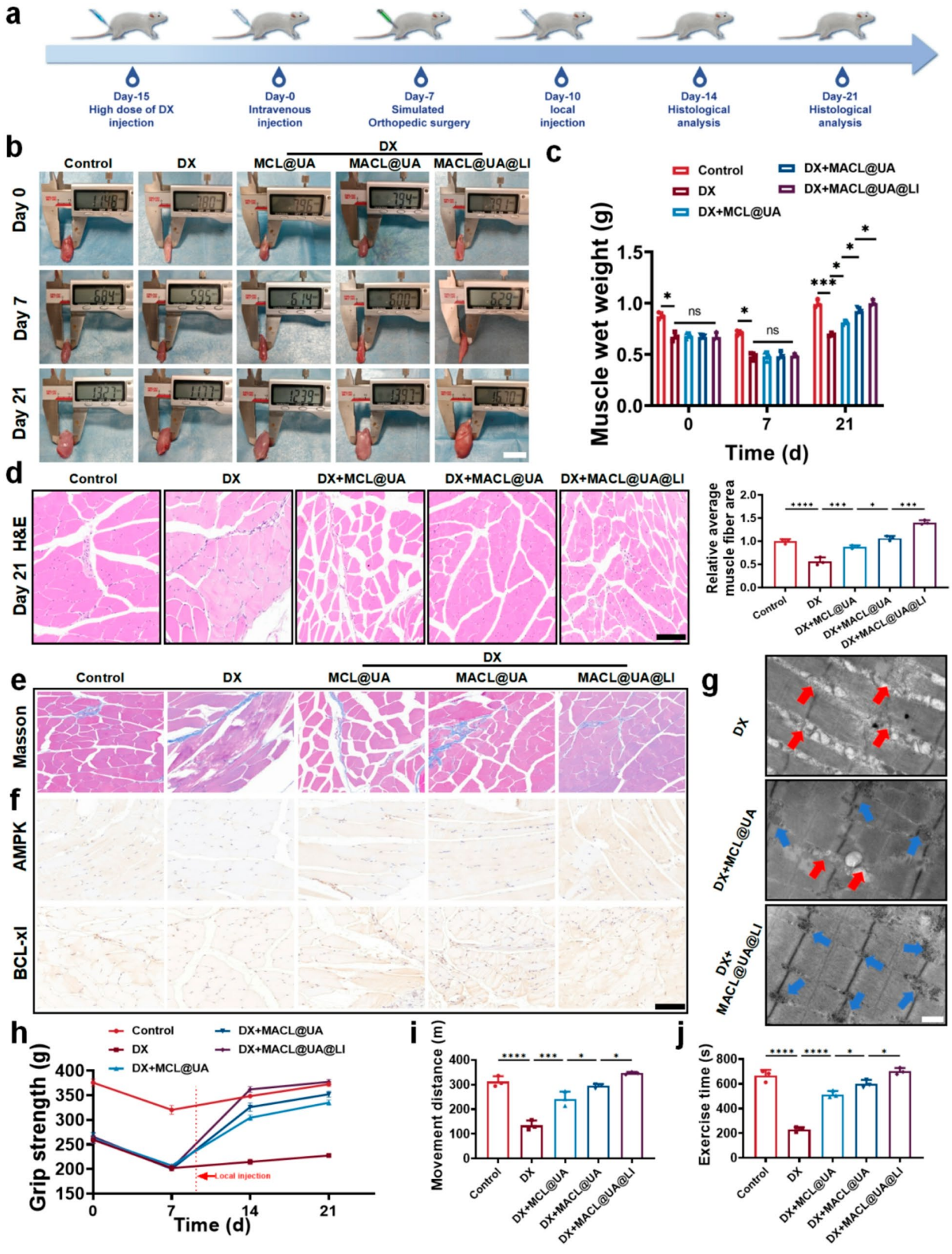

Fig. 7 (See legend on next page.)

(See figure on previous page.)

Fig. 7 Perioperative treatment of myasthenia gravis with MACL@UA. **a**) Establishment and steps of the perioperative model of sarcopenia. **b**) Measurement of muscle width of different treatment groups on day 0, 7 and 21. Scale bar, 20 mm. **c**) Muscle wet weight of rats in different treatment groups on day 0, 7 and 21. **d**) H&E staining images of muscles and quantitative analysis of mean muscle fiber area of different treatment groups on day 21. Scale bar, 200 μm. **e**) Masson staining images of different treatment groups. 200 μm. **f**) Immunohistochemical staining images of AMPK and BCL-xl. 200 μm. **g**) TEM images of muscle mitochondria after different treatments. Red arrows represent swollen mitochondria and blue arrows represent intact mitochondria. Scale bar, 10 μm. **h**) Grip force curves of rats after different treatments. **i**) Distance traveled and exercise time of rats measured by treadmill experiment. ($n = 3$, *$p < 0.05$, **$p < 0.01$, ***$p < 0.001$, ****$p < 0.0001$. Data are expressed in mean ± SD.)

no significant pathological changes or adverse reactions after MACL@UA injection, highlighting their high degree of histocompatibility (Figure S32).

According to the etiology and pathogenesis of myasthenia gravis, animal models of myasthenia gravis can be categorized into the following types: natural aging-related, drug-induced, exercise-deficient, nutritionally deficient and genetically engineered [76]. Laboratory animals can be used as natural aging myasthenia gravis models by keeping them in a normal environment until they reach a certain age, such as rats kept for more than 18 months. The limitations of this model are the long experimental period, the high cost, and the difficulty of controlling the differences between individuals, which may include genetic background, living environment, etc [77].

Drug-induced modeling is a common method of simulating or inducing a state of myasthenia gravis by means of a specific drug or chemical. Dexamethasone is a glucocorticoid that, when injected in high doses, inhibits the synthesis of muscle proteins and promotes their catabolism, leading to muscle atrophy. The main advantage is that aging-related changes can be observed in a relatively short period of time, but it may not fully reflect all the characteristics of natural aging [78].

Therefore, we selected rats of 18–20 months of age and injected DX at half the dose and half the course to produce a model of senile sarcopenia. Thus, we were able to maximize the control of individual differences in the natural aging-associated phenotype.

Conclusion

In this study, we developed a multifunctional myogenic nanomaterial, MACL@UA, for the treatment of systemic sarcopenia and orthopedic perioperative treatment. The release of large amounts of Mg^{2+} and UA from MACL@UA improved mitochondrial homeostasis and promoted myocyte proliferation. The release of Co^{2+} from MACL@UA facilitated angiogenesis and reconstruction. At the same time, the presence of Al regulated the metabolic crosstalk between macrophages and satellite cells, prompting macrophages to secrete large amounts of glutamine, which in turn nourished satellite cells. In vivo experiments have also demonstrated that MACL@UA has excellent therapeutic efficacy in the treatment of generalized systemic sarcopenia and orthopedic perioperative model. In conclusion. The excellent myogenic and vasculogenic capacity of MACL@UA provides new insights for the future treatment of generalized systemic sarcopenia and orthopedic perioperative therapy.

Supplementary Information

The online version contains supplementary material available at https://doi.org/10.1186/s12951-025-03480-1.

Supplementary Material 1

Acknowledgements
None.

Author contributions
Conceptualization: W.Z., C.Z., X.Z.Z., and J.M. Biomaterial preparation and characterization: P.W., Y.Z., Q.L., Q.M.L., and B.L.In vitro experiments: X.D.Z., Z.W., J.L.Animal experiments: X.D.Z., Z.W., J.L, and Q.L.Writing–original draft: X.D.Z. and Z.W. Writing–review, and editing: all authors. Supervision: W.Z. and X.Z.Z.

Funding
This work was supported by the National Natural Science Foundation of China (Grant No. 81871788, 82272512, 82102586, 82372427 and 82202672), the Key Research and Development Program of Anhui Province (No. 202004j07020013 and 2022e07020017), the Natural Science Foundation of Anhui Province (Grant No. 2108085QH319), the Fundamental Research Funds for the Central Universities (Grant No. WK9110000173 and WK9110000161), the Natural Science Foundation of Anhui Province, Distinguishing Youth Project (2108085J40), Anhui Provincial Key Research and Development Program-Clinical Medical Research Translation Specialization (202304295107020020), Research Funds of Centre for Leading Medicine and Advanced Technologies of IHM (2023IHM01070).

Data availability
No datasets were generated or analysed during the current study.

Declarations

Ethics approval and consent to participate
The animal experiments were approved by the Animal Care Committee of the First Affiliated Hospital of University of Science and Technology of China.

Consent for publication
Not applicable.

Competing interests
The authors declare no competing interests.

Author details
[1]Department of Orthopedics, Centre for Leading Medicine and Advanced Technologies of IHM, Division of Life Sciences and Medicine, The First Affiliated Hospital of USTC, University of Science and Technology of China, Hefei, Anhui 230001, China
[2]Department of Orthopedics, The Affiliated Provincial Hospital of Anhui Medical University, Anhui Medical University, Hefei, Anhui 230001, P. R. China
[3]Department of Orthopedics, Shanghai Sixth People's Hospital, Shanghai Jiao Tong University School of Medicine, Shanghai Jiao Tong University, Shanghai 200233, P. R. China

[4]Yichun University School of Medicine, No. 576 Yuanzhou District, Yichun, Jiangxi Province 336000, China
[5]Department of Orthopedics, Shanghai Tenth People's Hospital, Tongji University School of Medicine, No. 301 Yanchang Middle Road, Jing'an District, Shanghai 200072, China

Received: 8 September 2024 / Accepted: 24 February 2025
Published online: 28 May 2025

References

1. Vinciguerra M, Musaro A, Rosenthal N. Regulation of muscle atrophy in aging and disease. Adv Exp Med Biol. 2010;694:211–33.
2. Calvani R, Joseph AM, Adhihetty PJ, Miccheli A, Bossola M, Leeuwenburgh C, Bernabei R, Marzetti E. Mitochondrial pathways in sarcopenia of aging and disuse muscle atrophy. Biol Chem. 2013;394:393–414.
3. Bentzinger CF, Wang YX, Dumont NA, Rudnicki MA. Cellular dynamics in the muscle satellite cell niche. EMBO Rep. 2013;14:1062–72.
4. Liu D, Gao Y, Liu J, Huang Y, Yin J, Feng Y, Shi L, Meloni BP, Zhang C, Zheng M, Gao J. Intercellular mitochondrial transfer as a means of tissue revitalization. Signal Transduct Target Ther. 2021;6:65.
5. Romanello V, Sandri M. Mitochondrial quality control and muscle mass maintenance. Front Physiol. 2015;6:422.
6. Amigo I, da Cunha FM, Forni MF, Garcia-Neto W, Kakimoto PA, Luévano-Martínez LA, Macedo F, Menezes-Filho SL, Peloggia J, Kowaltowski AJ. Mitochondrial form, function and signalling in aging. Biochem J. 2016;473:3421–49.
7. Clark MA, Shay JW. Mitochondrial transformation of mammalian cells. Nature. 1982;295:605–7.
8. Guo Y, Chi X, Wang Y, Heng BC, Wei Y, Zhang X, Zhao H, Yin Y, Deng X. Mitochondria transfer enhances proliferation, migration, and osteogenic differentiation of bone marrow mesenchymal stem cell and promotes bone defect healing. Stem Cell Res Ther. 2020;11:245.
9. Hsu YC, Wu YT, Yu TH, Wei YH. Mitochondria in mesenchymal stem cell biology and cell therapy: from cellular differentiation to mitochondrial transfer. Semin Cell Dev Biol. 2016;52:119–31.
10. Islam MN, Das SR, Emin MT, Wei M, Sun L, Westphalen K, Rowlands DJ, Quadri SK, Bhattacharya S, Bhattacharya J. Mitochondrial transfer from bone-marrow-derived stromal cells to pulmonary alveoli protects against acute lung injury. Nat Med. 2012;18:759–65.
11. Caicedo A, Aponte PM, Cabrera F, Hidalgo C, Khoury M. Artificial mitochondria transfer: current challenges, advances, and future applications. Stem Cells Int. 2017;2017:7610414.
12. Caldeira DAF, de Oliveira DF, Cavalcanti-de-Albuquerque JP, Nascimento JHM, Zin WA, Maciel L. Isolation of mitochondria from fresh mice lung tissue. Front Physiol. 2021;12:748261.
13. Vasan K, Werner M, Chandel NS. Mitochondrial metabolism as a target for Cancer therapy. Cell Metab. 2020;32:341–52.
14. Wu TH, Sagullo E, Case D, Zheng X, Li Y, Hong JS, TeSlaa T, Patananan AN, McCaffery JM, Niazi K, et al. Mitochondrial transfer by photothermal nanoblade restores metabolite profile in mammalian cells. Cell Metab. 2016;23:921–9.
15. Reddy P, Ocampo A, Suzuki K, Luo J, Bacman SR, Williams SL, Sugawara A, Okamura D, Tsunekawa Y, Wu J, et al. Selective elimination of mitochondrial mutations in the germline by genome editing. Cell. 2015;161:459–69.
16. Taanman JW. The mitochondrial genome: structure, transcription, translation and replication. Biochim Biophys Acta. 1999;1410:103–23.
17. Huang L, Reis C, Boling WW, Zhang JH. Stem cell therapy in brain ischemia: the role of mitochondrial transfer. Stem Cells Dev. 2020;29:555–61.
18. Huang T, Zhang T, Jiang X, Li A, Su Y, Bian Q, Wu H, Lin R, Li N, Cao H, et al. Iron oxide nanoparticles augment the intercellular mitochondrial transfer-mediated therapy. Sci Adv. 2021;7:eabj0534.
19. Palanisami A, Fang J, Lowder TW, Kunz H, Miller JH Jr. Rapid morphological characterization of isolated mitochondria using brownian motion. Anal Methods. 2012;4:513–21.
20. Patananan AN, Sercel AJ, Wu TH, Ahsan FM, Torres A Jr., Kennedy SAL, Vandiver A, Collier AJ, Mehrabi A, Van Lew J, et al. Pressure-Driven mitochondrial transfer pipeline generates mammalian cells of desired genetic combinations and fates. Cell Rep. 2020;33:108562.
21. Patananan AN, Wu TH, Chiou PY, Teitell MA. Modifying the mitochondrial genome. Cell Metab. 2016;23:785–96.
22. Smythe GM, Hodgetts SI, Grounds MD. Immunobiology and the future of myoblast transfer therapy. Mol Ther. 2000;1:304–13.
23. Saclier M, Cuvellier S, Magnan M, Mounier R, Chazaud B. Monocyte/macrophage interactions with myogenic precursor cells during skeletal muscle regeneration. Febs J. 2013;280:4118–30.
24. Shen J, Zhu X, Liu H. MiR-483 induces senescence of human adipose-derived mesenchymal stem cells through IGF1 Inhibition. Aging. 2020;12:15756–70.
25. Wang Y, Jin R, Shen B, Li N, Zhou H, Wang W, Zhao Y, Huang M, Fang P, Wang S et al. High-throughput functional screening for next-generation cancer immunotherapy using droplet-based microfluidics. Sci Adv 2021, 7.
26. Juhas M, Abutaleb N, Wang JT, Ye J, Shaikh Z, Sriworarat C, Qian Y, Bursac N. Incorporation of macrophages into engineered skeletal muscle enables enhanced muscle regeneration. Nat Biomed Eng. 2018;2:942–54.
27. Rennie MJ, MacLennan PA, Hundal HS, Weryk B, Smith K, Taylor PM, Egan C, Watt PW. Skeletal muscle glutamine transport, intramuscular glutamine concentration, and muscle-protein turnover. Metabolism. 1989;38:47–51.
28. Ahmed F, Zviedrite N, Uzicanin A. Effectiveness of workplace social distancing measures in reducing influenza transmission: a systematic review. BMC Public Health. 2018;18:518.
29. Minczuk M, Papworth MA, Kolasinska P, Murphy MP, Klug A. Sequence-specific modification of mitochondrial DNA using a chimeric zinc finger Methylase. Proc Natl Acad Sci U S A. 2006;103:19689–94.
30. Patel D, Rorbach J, Downes K, Szukszto MJ, Pekalski ML, Minczuk M. Macropinocytic entry of isolated mitochondria in epidermal growth factor-activated human osteosarcoma cells. Sci Rep. 2017;7:12886.
31. Gharibi B, Farzadi S, Ghuman M, Hughes FJ. Inhibition of Akt/mTOR attenuates age-related changes in mesenchymal stem cells. Stem Cells. 2014;32:2256–66.
32. Shadel GS, Horvath TL. Mitochondrial ROS signaling in organismal homeostasis. Cell. 2015;163:560–9.
33. Barciszewski J, Szpotkowski K, Wisniewski J, Kolodziejczyk R, Rakus D, Jaskolski M, Dzugaj A. Structural studies of human muscle FBPase. Acta Biochim Pol. 2021;68:5–14.
34. Fang J, Sia J, Soto J, Wang P, Li LK, Hsueh YY, Sun R, Faull KF, Tidball JG, Li S. Skeletal muscle regeneration via the chemical induction and expansion of myogenic stem cells in situ or in vitro. Nat Biomed Eng. 2021;5:864–79.
35. Bian Y, Cai X, Lv Z, Xu Y, Wang H, Tan C, Liang R, Weng X. Layered double hydroxides: A novel promising 2D nanomaterial for bone diseases treatment. Adv Sci (Weinh). 2023;10:e2301806.
36. Konishi M. Cytoplasmic free concentrations of Ca2 + and Mg2 + in skeletal muscle fibers at rest and during contraction. Jpn J Physiol. 1998;48:421–38.
37. Konishi M, Suda N, Kurihara S. Fluorescence signals from the Mg2+/Ca2 + indicator Furaptra in frog skeletal muscle fibers. Biophys J. 1993;64:223–39.
38. Lamb GD, Stephenson DG. Effect of Mg2 + on the control of Ca2 + release in skeletal muscle fibres of the Toad. J Physiol. 1991;434:507–28.
39. Burdzińska A, Gala K, Paczek L. Myogenic stem cells. Folia Histochem Cytobiol. 2008;46:401–12.
40. Zammit PS. Function of the myogenic regulatory factors Myf5, MyoD, Myogenin and MRF4 in skeletal muscle, satellite cells and regenerative myogenesis. Semin Cell Dev Biol. 2017;72:19–32.
41. Huang Z, Zhang Y, Liu R, Li Y, Rafique M, Midgley AC, Wan Y, Yan H, Si J, Wang T, et al. Cobalt loaded electrospun poly(ε-caprolactone) grafts promote antibacterial activity and vascular regeneration in a diabetic rat model. Biomaterials. 2022;291:121901.
42. Francis WR, Liu Z, Owens SE, Wang X, Xue H, Lord A, Kanamarlapudi V, Xia Z. Role of hypoxia inducible factor 1α in Cobalt nanoparticle induced cytotoxicity of human THP-1 macrophages. Biomater Transl. 2021;2:143–50.
43. Shu C, Qin C, Wu A, Wang Y, Zhao C, Shi Z, Niu H, Chen J, Huang J, Zhang X, et al. 3D printing of Cobalt-Incorporated chloroapatite bioceramic composite scaffolds with antioxidative activity for enhanced osteochondral regeneration. Adv Healthc Mater. 2024;13:e2303217.
44. Gu M, Wei Z, Wang X, Gao Y, Wang D, Liu X, Bai C, Su G, Yang L, Li G. Myostatin knockout affects mitochondrial function by inhibiting the AMPK/SIRT1/PGC1α pathway in skeletal muscle. Int J Mol Sci 2022, 23.
45. Guo A, Li K, Tian HC, Fan Z, Chen QN, Yang YF, Yu J, Wu YX, Xiao Q. FGF19 protects skeletal muscle against obesity-induced muscle atrophy, metabolic derangement and abnormal Irisin levels via the AMPK/SIRT-1/PGC-α pathway. J Cell Mol Med. 2021;25:3585–600.
46. Zhou X, Xu S, Zhang Z, Tang M, Meng Z, Peng Z, Liao Y, Yang X, Nüssler AK, Liu L, Yang W. Gouqi-derived nanovesicles (GqDNVs) inhibited

dexamethasone-induced muscle atrophy associating with AMPK/SIRT1/PGC1α signaling pathway. J Nanobiotechnol. 2024;22:276.
47. Yu X, Wang Y, Ran L, Jiang Y, Chen M, Du H, Zhang Y, Wu D, Xiang X, Zhang J, et al. Tetrahedral framework nucleic acids inhibit muscular Mitochondria-Mediated apoptosis and ameliorate muscle atrophy in sarcopenia. Nano Lett. 2023;23:8816–26.
48. Li X, Aghaamoo M, Liu S, Lee DH, Lee AP. Lipoplex-Mediated Single-Cell transfection via droplet microfluidics. Small. 2018;14:e1802055.
49. Mazutis L, Gilbert J, Ung WL, Weitz DA, Griffiths AD, Heyman JA. Single-cell analysis and sorting using droplet-based microfluidics. Nat Protoc. 2013;8:870–91.
50. Picard M, Zhang J, Hancock S, Derbeneva O, Golhar R, Golik P, O'Hearn S, Levy S, Potluri P, Lvova M, et al. Progressive increase in MtDNA 3243A > G heteroplasmy causes abrupt transcriptional reprogramming. Proc Natl Acad Sci U S A. 2014;111:E4033–4042.
51. Steinberg GR, Hardie DG. New insights into activation and function of the AMPK. Nat Rev Mol Cell Biol. 2023;24:255–72.
52. Li X, Zhu W, Liu R, Ding G, Huang H. Cerium oxide nanozymes improve skeletal muscle function in gestational diabetic offspring by attenuating mitochondrial oxidative stress. ACS Omega. 2024;9:21851–63.
53. Lv T, Fan X, He C, Zhu S, Xiong X, Yan W, Liu M, Xu H, Shi R, He Q. SLC7A11-ROS/αKG-AMPK axis regulates liver inflammation through mitophagy and impairs liver fibrosis and NASH progression. Redox Biol. 2024;72:103159.
54. Jiang P, Ren L, Zhi L, Yu Z, Lv F, Xu F, Peng W, Bai X, Cheng K, Quan L, et al. Negative regulation of AMPK signaling by high glucose via E3 ubiquitin ligase MG53. Mol Cell. 2021;81:629–e637625.
55. Cheng D, Zhang M, Zheng Y, Wang M, Gao Y, Wang X, Liu X, Lv W, Zeng X, Belosludtsev KN, et al. α-Ketoglutarate prevents hyperlipidemia-induced fatty liver mitochondrial dysfunction and oxidative stress by activating the AMPK-pgc-1α/Nrf2 pathway. Redox Biol. 2024;74:103230.
56. Bawazer LA, McNally CS, Empson CJ, Marchant WJ, Comyn TP, Niu X, Cho S, McPherson MJ, Binks BP, deMello A, Meldrum FC. Combinatorial microfluidic droplet engineering for biomimetic material synthesis. Sci Adv. 2016;2:e1600567.
57. Gao J, Qin A, Liu D, Ruan R, Wang Q, Yuan J, Cheng TS, Filipovska A, Papadimitriou JM, Dai K, et al. Endoplasmic reticulum mediates mitochondrial transfer within the osteocyte dendritic network. Sci Adv. 2019;5:eaaw7215.
58. Joseph AM, Adhihetty PJ, Leeuwenburgh C. Beneficial effects of exercise on age-related mitochondrial dysfunction and oxidative stress in skeletal muscle. J Physiol. 2016;594:5105–23.
59. Di Carlo D, Irimia D, Tompkins RG, Toner M. Continuous inertial focusing, ordering, and separation of particles in microchannels. Proc Natl Acad Sci U S A. 2007;104:18892–7.
60. Ghazimirsaeed E, Madadelahi M, Dizani M, Shamloo A. Secondary flows, mixing, and chemical reaction analysis of Droplet-Based flow inside serpentine microchannels with different cross sections. Langmuir. 2021;37:5118–30.
61. Kitani T, Kami D, Matoba S, Gojo S. Internalization of isolated functional mitochondria: involvement of macropinocytosis. J Cell Mol Med. 2014;18:1694–703.
62. Manatunga DC, Godakanda VU, de Silva RM, de Silva KMN. Recent developments in the use of organic-inorganic nanohybrids for drug delivery. Wiley Interdiscip Rev Nanomed Nanobiotechnol. 2020;12:e1605.
63. Song H, Tice JD, Ismagilov RF. A microfluidic system for controlling reaction networks in time. Angew Chem Int Ed Engl. 2003;42:768–72.
64. Del Prete Z, Musarò A, Rizzuto E. Measuring mechanical properties, including isotonic fatigue, of fast and slow MLC/mIgf-1 Transgenic skeletal muscle. Ann Biomed Eng. 2008;36:1281–90.
65. King MP, Attardi G. Injection of mitochondria into human cells leads to a rapid replacement of the endogenous mitochondrial DNA. Cell. 1988;52:811–9.
66. Briggs D, Morgan JE. Recent progress in satellite cell/myoblast engraftment -- relevance for therapy. Febs J. 2013;280:4281–93.
67. Yang J, Zhang X, Lu B, Mei J, Xu L, Zhang X, Su Z, Xu W, Fang S, Zhu C, et al. Inflammation-Responsive hydrogel spray for synergistic prevention of traumatic heterotopic ossification via Dual-Homeostatic modulation strategy. Adv Sci (Weinh). 2023;10:e2302905.
68. Jeske R, Yuan X, Fu Q, Bunnell BA, Logan TM, Li Y. In vitro culture expansion shifts the immune phenotype of human Adipose-Derived mesenchymal stem cells. Front Immunol. 2021;12:621744.
69. Karaki H. Magnesium as a modifier of smooth muscle contractility. Microcirc Endothelium Lymphatics. 1989;5:77–97.
70. Zheng B, Wang Y, Zhou B, Qian F, Liu D, Ye D, Zhou X, Fang L. Urolithin A inhibits breast cancer progression via activating TFEB-mediated mitophagy in tumor macrophages. J Adv Res 2024.
71. Kuerec AH, Lim XK, Khoo AL, Sandalova E, Guan L, Feng L, Maier AB. Targeting aging with urolithin A in humans: A systematic review. Ageing Res Rev. 2024;100:102406.
72. Rives V, Del Arco M, Martín C. Layered double hydroxides as drug carriers and for controlled release of non-steroidal antiinflammatory drugs (NSAIDs): a review. J Control Release. 2013;169:28–39.
73. Shang M, Cappellesso F, Amorim R, Serneels J, Virga F, Eelen G, Carobbio S, Rincon MY, Maechler P, De Bock K, et al. Macrophage-derived glutamine boosts satellite cells and muscle regeneration. Nature. 2020;587:626–31.
74. Qazi TH, Duda GN, Ort MJ, Perka C, Geissler S, Winkler T. Cell therapy to improve regeneration of skeletal muscle injuries. J Cachexia Sarcopenia Muscle. 2019;10:501–16.
75. Behrens A, van Deursen JM, Rudolph KL, Schumacher B. Impact of genomic damage and ageing on stem cell function. Nat Cell Biol. 2014;16:201–7.
76. Christian CJ, Benian GM. Animal models of sarcopenia. Aging Cell. 2020;19:e13223.
77. Nemoto A, Goyagi T. Tail suspension is useful as a sarcopenia model in rats. Lab Anim Res. 2021;37:7.
78. Xie WQ, He M, Yu DJ, Wu YX, Wang XH, Lv S, Xiao WF, Li YS. Mouse models of sarcopenia: classification and evaluation. J Cachexia Sarcopenia Muscle. 2021;12:538–54.

Publisher's note